Long-range, short-wavelength, and ultrafast heat conduction driven by three plasmon modes supported by graphene

Jose Ordonez-Miranda [1,2,*] Yuriy A. Kosevich [3,2] Masahiro Nomura [2,1] and Sebastian Volz [1,2]

[1]*LIMMS, CNRS-IIS IRL 2820, The University of Tokyo, Tokyo 153-8505, Japan*
[2]*Institute of Industrial Science, The University of Tokyo, Tokyo 153-8505, Japan*
[3]*N. N. Semenov Federal Research Center for Chemical Physics of Russian Academy of Sciences,
4 Kosygin Street, Moscow 119991, Russian Federation*

We demonstrate the existence and propagation of three hybrid modes of surface plasmon polaritons supported by two graphene monolayers coating a solid film. These modes propagate long distances with short wavelengths, which are suitable features to enhance the heat conduction along the film interfaces. For a Si film with a thickness of 15 nm and a length of 5 mm at 300 K, we find a plasmon thermal conductivity of $13.6 \, \text{W} \, \text{m}^{-1} \, \text{K}^{-1}$, which represents 67% (26%) of its phonon Si (Si+graphene) counterpart. This thermal energy appears due to the coupling of plasmons propagating at speeds comparable to the speed of light in vacuum. The plasmonic heat conduction driven by two-dimensional materials thus appears as a major and unexpected mechanism for controlling temperature in solid-state systems at rates faster than the ones of phonons and electrons.

Heat dissipation in dielectrics is mainly driven by acoustic phonons with a long mean free path and high group velocity as compared with those of optical phonons. Even though optical phonons have larger heat capacities than the acoustic ones, their ability to dissipate heat is limited by their localized nature and low speeds. In polar dielectrics, however, the optical phonons support the propagation of surface phonon polaritons (SPhPs), which are electromagnetic waves confined to the material interface [1–6]. The in-plane propagation and cross-plane evanescent nature of these surface waves enable them to propagate distances (>1 mm) much greater than the typical mean free path of phonons and electrons [7,8] and hence their guiding along interfaces can generate an efficient channel of heat conduction [9–11].

Previous theoretical [1,2] and experimental [9,10,12,13] works reported that the SPhP contribution to the in-plane thermal conductivity of polar nanofilms can be comparable to or higher than its phonon counterpart. This thermal performance enhancement arises from the coupling of a single SPhP mode propagating along the two nanofilm interfaces [1,2]. The SPhP coupling also appears in microsized structures made up of a thick Si layer sandwiched by polar nanolayers [14]. The weak energy absorption in this symmetric structure support the propagation of multiple SPhP modes, which can enhance the in-plane SPhP heat transport to values ten times higher than the corresponding one of a single polar nanofilm [14,15]. As the Si thickness scales down, the number of these SPhP modes reduces and reaches its minimum of two modes for nanoscales. This is also the case of surface plasmon polaritons (SPPs) generated by the hybridization of

photons and free electrons in metallic nanofilms. The plasmonic heat conduction along these nanofilms is driven by two fundamental plasmon modes [16,17], whose contribution to significantly boost the in-plane thermal conductivity of a Ti nanofilm was recently observed experimentally [18]. These works [15,16,18] suggest that the plasmonic heat conduction could naturally be enhanced via highly conductive two-dimensional (2D) materials. Even though the electron thermal conductivity of graphene has been widely studied [19–23] along with its ability to support plasmon modes [24–26], their contribution to the heat conduction is not known yet. As the number of these modes can be multiplied by coating a solid with graphene, they have the potential to enhance the thermal performance of solids, without changing their internal material structure.

The purpose of this Letter is to demonstrate the potential of 2D materials for enhancing heat conduction currents. For a film coated with a 2D material, we show that this current is driven by three ultrafast modes featuring long propagation distances and short wavelengths. These features allow them to significantly enhance the thermal performance of a graphene-coated nanofilm.

Let us consider a suspended film supporting the propagation of SPPs along its two interfaces coated with graphene monolayers, as shown in Fig. 1. The film and its surrounding medium have relative permittivities ε_1 and ε_2, respectively. Considering that the film surfaces $x = 0$ and $x = l$ are in contact with thermal baths at temperatures T_h and $T_c (< T_h)$, the free electrons of graphene oscillate and emit an electromagnetic field. These oscillations induce the excitation of neighboring electrons, which keeps the field propagation mainly along the film interfaces. This thermally excited field represents a SPP propagating in a broad range of frequency [18,25,27]. Under this condition, the heat propagates along
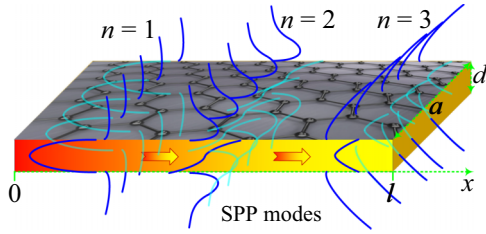
*jose.ordonez@cnrs.fr

FIG. 1. Scheme of a film supporting the propagation of three SPP modes. The curvy lines stand for the SPP magnetic field, whose discontinuity at the film interfaces appears due to their coating with a graphene monolayer.

the x axis mostly via the combined dynamics of the film phonons (or electrons) and SPPs. Given that SPPs are bosons [6], the Boltzmann transport equation establishes that their contribution k to the in-plane thermal conductivity of the film is given by [4]

$$k = \frac{1}{4\pi d} \int \hbar\omega \, \text{Re}(\beta) \Lambda_e \frac{\partial f}{\partial T} d\omega, \qquad (1)$$

where $\hbar$ is the Planck's constant divided by 2π, $\text{Re}(\beta)$ is the real part of the in-plane SPP wave vector β, $f = [\exp(\hbar\omega/k_B T) - 1]^{-1}$ is the Bose-Einstein distribution, $T = (T_h + T_c)/2$ is the average temperature, k_B is the Boltzmann constant, ω is the spectral frequency, and Λ_e is the effective propagation length defined by [4]

$$\Lambda_e = \Lambda \left[1 - \frac{4}{\pi\mu} \left(\frac{2}{3} - E_5(\mu) \right) \right], \qquad (2)$$

where $\mu = l/\Lambda$, $\Lambda = [2\,\text{Im}(\beta)]^{-1}$ is the intrinsic SPP propagation length, l is the film length, and $E_5(x) = \int_0^{\pi/2} \cos^3(\theta) e^{-x/\cos(\theta)} d\theta$. The effective propagation length Λ_e represents the distance that SPPs can travel along the film interfaces and therefore its values are comparable to or smaller than l and Λ. In the diffusive regime ($\mu = l/\Lambda \gg 1$), $\Lambda_e = \Lambda$, and Eq. (2) reduces to the previous one derived by Chen *et al.* [1]. By contrast, for the ballistic limit ($\mu \ll 1$), the SPP propagation is limited by the film length and $\Lambda_e = 2l/\pi$. The SPP heat transport is hence enhanced along a film with length smaller than the SPP propagation length ($l \ll \Lambda$). For an arbitrary $\Lambda_e = \Lambda_e(\Lambda, l)$, Eqs. (1) and (2) show that k depends on the material properties through the product $\text{Re}(\beta)\Lambda_e[0.5/\text{Im}(\beta), l]$ driven by the real and imaginary parts of the SPP wave vector $\beta(\omega)$. As k increases with this product, the optimal material configuration to maximize the SPP heat transport is given by a large wave vector $\text{Re}(\beta)$ [short wavelength $2\pi/\text{Re}(\beta)$] and a long propagation length [small $\text{Im}(\beta)$]. The predictions of Eq. (1) derived from the Boltzmann transport equation agree with the corresponding ones of the fluctuational electrodynamics theory [28] and describe well experimental data for the thermal conductivity of SiO_2 and SiN nanofilms [9,10]. After solving the Maxwell equations for the transverse magnetic polarization required for the existence of SPPs, the following two dispersion relations for

$\beta(\omega)$ are obtained [29],

$$\frac{\varepsilon_2}{p_2} + \frac{\varepsilon_1}{p_1} \coth(p_1 d/2) = -\frac{i\sigma}{\omega\varepsilon_0}, \qquad (3a)$$

$$\frac{\varepsilon_2}{p_2} + \frac{\varepsilon_1}{p_1} \tanh(p_1 d/2) = -\frac{i\sigma}{\omega\varepsilon_0}, \qquad (3b)$$

where $i = \sqrt{-1}$ is the imaginary unit, ε_0 is the vacuum permittivity, σ is the 2D electrical conductivity of a graphene monolayer, and p_n are the cross-plane wave vectors given by $p_n^2 = \beta^2 - \varepsilon_n k_0^2$, with $k_0 = \omega/c$ and c being the wave vector and speed of light in vacuum, respectively. The modes in Eqs. (3a) and (3b) describe the SPP propagation with a respective symmetric $[H_y(-z) = H_y(z)]$ and antisymmetric $[H_y(-z) = -H_y(z)]$ magnetic field, as detailed in the Supplemental Material (SM) [29]. For a very thick film ($|p_2|d \gg 2$), both Eqs. (3a) and (3b) become independent of the film thickness and reduce to the well-known dispersion relation $\varepsilon_1/p_1 + \varepsilon_2/p_2 = -i\sigma/(\omega\varepsilon_0)$ of a single interface [2]. For very thin films ($|p_2|d \ll 2$), on the other hand, the solution of Eqs. (3a) and (3b) for $\beta = k_0\sqrt{\varepsilon}$ can conveniently be found in terms of the effective permittivity ε and the normalized thickness $\lambda = k_0 d/2 \ll 1$, as detailed in the SM [29]. For an approximation up to λ^2, the solutions $n = 1$ and $n = 2$ thus obtained for Eqs. (3a) and (3b) are respectively given by

$$\varepsilon = \frac{i\varepsilon_1}{S\lambda} + \frac{i\varepsilon_2}{S}\sqrt{\frac{i\varepsilon_1}{S\lambda}} + \varepsilon_1 - \frac{1}{S^2}\left(\frac{\varepsilon_1^2}{3} + \frac{\varepsilon_2^2}{2}\right), \qquad (4a)$$

$$\varepsilon = \varepsilon_2 - \left(\frac{\varepsilon_2}{S}\right)^2\left[1 + 2i\frac{\varepsilon_1\lambda}{S} - 3\left(\frac{\varepsilon_1\lambda}{S}\right)^2\right], \qquad (4b)$$

where $S = \sigma/(c\varepsilon_0) \neq 0$ is the normalized and dimensionless electrical conductivity of graphene. Since $\lambda \ll 1$, the leading term in Eq. (4a) indicates that the mode $n = 1$ features a large wave vector $\text{Re}(\beta) \rightarrow d^{-1/2}$ and a small propagation length $\Lambda \rightarrow d^{1/2}$. These short-wavelength and short-range SPPs appear due to the increasing energy absorption of graphene, as the film thickness scales down. For this branch $n = 1$, the SPP propagations along the in-plane and cross-plane directions are driven by the same wave vectors ($\beta \approx p_1 \approx p_2$) [29]. For mode $n = 2$, on the other hand, $\beta \rightarrow k_0\sqrt{\varepsilon_2 - (\varepsilon_2/S)^2}$ becomes independent of the film thickness and permittivity, for thin enough films. Therefore, the coupling of the SPP mode $n = 2$ propagating along the two film interfaces saturates, as the film thickness sizes down. Note that both modes $n = 1$ and $n = 2$ exist due to the presence of graphene ($S \neq 0$) and they are respectively driven by the media permittivities $\varepsilon \rightarrow \varepsilon_1$ and $\varepsilon \rightarrow \varepsilon_2$, for a very high conductivity $S \rightarrow \infty$. Both modes can thus exist even if the film and its surrounding medium are made of the same material ($\varepsilon_1 = \varepsilon_2$). However, as a result of the permittivity difference $\varepsilon_1 - \varepsilon_2 \neq 0$, Eq. (3a) predicts the propagation of a third mode ($n = 3$) determined by

$$\varepsilon = \varepsilon_2 + \left(1 - \frac{\varepsilon_2}{\varepsilon_1}\right)^2 (\varepsilon_2\lambda)^2\left[1 + 2i\left(1 - \frac{\varepsilon_2}{\varepsilon_1}\right)S\lambda\right]. \qquad (5)$$

The leading dependence of this third mode on the graphene conductivity is thus weighted by the normalized thickness λ to the third power. This weak dependence of ε on S indicates that the mode $n = 3$ is not strongly affected by the graphene energy absorption and therefore it can propagate
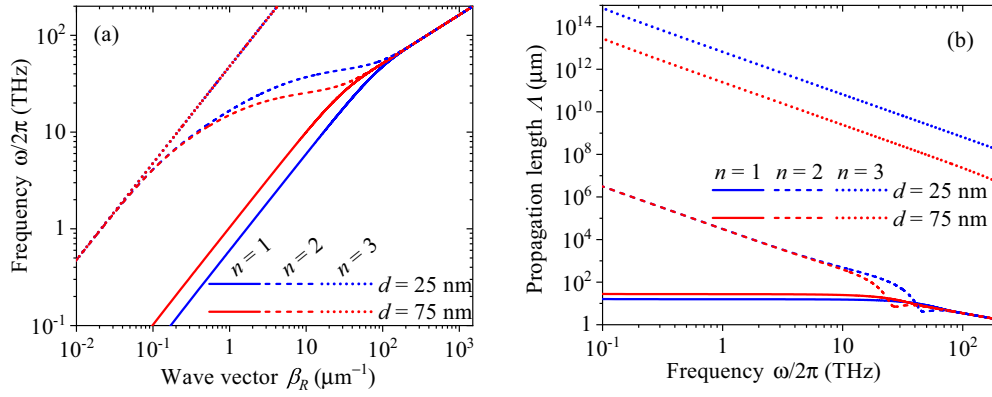
FIG. 2. Spectra of the in-plane (a) wave vector and (b) propagation length of the three SPP modes propagating along a graphene-coated Si film with $d = 25$ and 75 nm.

long distances, in absence of energy absorption by the film and its surrounding medium [$\text{Im}(\varepsilon_1) = \text{Im}(\varepsilon_2) = 0$]. As the SPP thermal conductivity increases with the SPP propagation length, this third mode is expected to significantly enhance the heat transport along the film interfaces, as confirmed below. Therefore, while the propagation of the first two modes is driven by either the permittivity of the film or its surrounding medium, mainly, the third mode is driven by the permittivity difference of these media.

We now determine numerically the propagation and thermal properties of SPPs propagating along a Si film ($\varepsilon_1 = 11.7$) surrounded by air ($\varepsilon_2 = 1$). These two media do not absorb energy in a large frequency range [30] and therefore they favor the propagation of SPPs over long distances. In addition, considering that the Si permittivity only increases slightly with temperature [30,31], for the considered range of temperatures [(300; 700) K], we assume its behavior is well represented by its given mean value. The graphene monolayers on the top and bottom surfaces of the film are good SPP conductors that absorb energy and hence support the SPP heat transport. For temperatures comparable to or higher than 300 K, the 2D conductivity σ of a graphene monolayer can be described by the following Drude-like model,

$$\sigma = \frac{\Omega}{\gamma - i\omega}, \tag{6}$$

where γ is the electron scattering rate and $\Omega = (e/\hbar)^2 E_F/\pi$, with e and E_F being the electron charge and Fermi energy, respectively. σ is thus determined by two parameters, whose estimated experimental values are $\gamma/2\pi = 1.59$ THz and $E_F = 1$ eV [24,26]. As the chemical potential E_F drives the density of free carriers, the proportionality $\sigma \propto E_F$ and the dispersion relations in Eqs. (3a) and (3b) indicate that the plasmon heat conduction increases with E_F. Equation (6) represents the intraband contribution to σ, as the interband one becomes negligible for $\hbar\omega < 2E_F$ ($\omega/2\pi < 483$ THz) [24,25,32]. This frequency interval covers the vast majority of relevant frequencies for the propagation and heat conduction of plasmons, for temperatures from 300 to 700 K, as shown below.

The in-plane wave vector β_R and propagation length Λ of SPPs propagating along a graphene-coated Si film are shown

in Figs. 2(a) and 2(b), respectively. Mode $n = 1$ [Eq. (4a)] exhibits the largest β_R (shortest wavelength) and smallest Λ, which takes values below 30 μm. The wave vector of mode $n = 1$ increases with frequency and takes higher values for thinner films, while its propagation length exhibits the opposite behavior. This short-wavelength mode ($n = 1$) is therefore expected to contribute to the SPP heat transport due to its large wave vector, which is nearly two orders of magnitude larger than that of mode $n = 3$. For mode $n = 3$, β_R linearly increases with frequency and is very close to the wave vector of light in vacuum ($\beta_R \approx k_0$). This photonlike nature of SPPs is accompanied by very long propagation lengths resulting from the weak energy absorption of graphene [see Eq. (5)]. The major contribution of mode $n = 3$ to the SPP heat transport is thus expected to arise from its long propagation length. Mode $n = 2$, on the other hand, has intermediate wave vectors and propagation lengths, whose values are between the corresponding ones of the other two modes. In contrast to mode $n = 1$, these two propagation parameters of mode $n = 2$ are nearly independent of the film thickness, for frequencies lower than 10 THz, as established by its weak dependence on d [see Eq. (4b)]. According to Fig. 2(a), the three modes propagate with a group velocity $V_g = \partial\omega/\partial\beta_R$ near to the speed of light in vacuum (see SM [29]) and hence they can drive a plasmonic heat conduction much faster than those of phonons and electrons.

The propagation length of the three SPP modes has a similar behavior than the SPP skin depth $\delta_1 = [2\,\text{Re}(p_1)]^{-1}$ inside the Si film, as shown in Fig. 3(a). The SPP energy absorption by the film hence reduces both the in-plane (Λ) and cross-plane (δ_1) propagation distances of SPPs. For a given frequency, the intrafilm skin depth satisfies the relation $\delta_1(n = 1) < \delta_1(n = 2) < \delta_1(n = 3)$ and its values are generally longer than the film thickness ($\delta_1 > d$). The SPPs propagating along the bottom and top film surfaces are thus coupled and exist in a broad band of frequencies. This existence is further confirmed by the spatial distribution of the Poynting vector shown in Fig. 3(b). The energy density of modes $n = 1$ and 2 is confined mainly along the film interfaces, while the intrafilm energy of $n = 3$ is much smaller the extra-film one, due to the high sensitivity of this third mode to the permittivity of the nonabsorbing air [see Eq. (4b)].
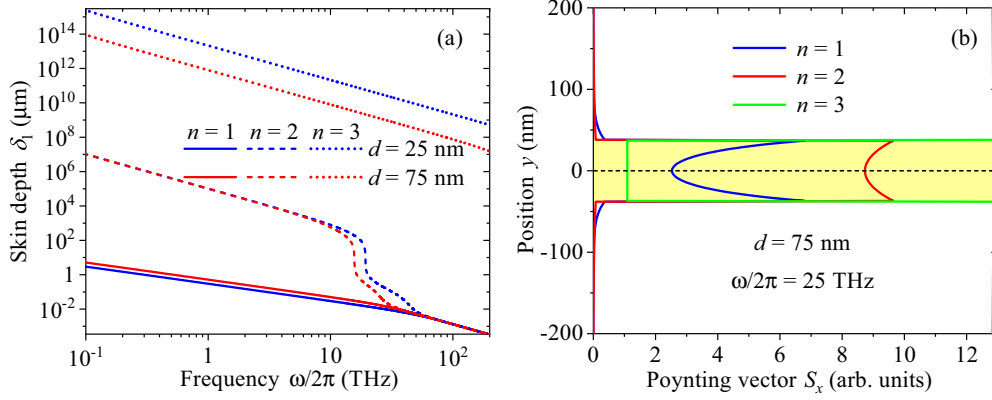
FIG. 3. (a) Spectrum of the cross-plane propagation length of the three SPP modes and (b) spatial distribution of the in-plane component of their Poynting vector.

The contributions of the three SPP modes to the spectrum k_ω of the SPP thermal conductivity [$k = \int k_\omega d\omega$ in Eq. (1)] of the graphene-coated Si film are shown in Fig. 4(a). The maxima of k_ω and their frequencies of occurrence increase as the film thickness decreases, such that $k_\omega(n = 1) > k_\omega(n = 3) > k_\omega(n = 2)$. The short-wavelength mode ($n = 1$) thus carries more thermal energy than the long-range one ($n = 3$), as a result of the limited length ($l = 1$ mm) of the considered film. Mode $n = 2$ exhibits the lowest contribution because the peak of k_ω results from the maximization of both β_R and Λ, which take intermediate values only, as shown in Fig. 2. For frequencies higher than the peak ones, the sharp reduction of k_ω is driven by the exponential decrease of the Bose-Einstein distribution function [see Eq. (1)], such that its values nearly vanish for $\omega/2\pi > 100$ THz. The three SPP modes thus exhibit broad frequency spectra and their contribution to the SPP thermal conductivity fulfill the relation $k(n = 1) > k(n = 3) > k(n = 2)$, as shown in Fig. 4(b). The near-linear increase of k with temperature deviates from the quadratic one predicted for the ballistic regime ($l \ll \Lambda$) in polar films [4], because the propagation length of modes $n = 1$ and $n = 2$ shown in Fig. 2(b) takes smaller and greater values than the film length $l = 1$ mm. Therefore, in the ballistic-diffusive regime, the SPP thermal conductivity increases with temperature slower than in the pure ballistic one.

The sum of the contributions of the three SPP modes to the SPP thermal conductivity k of the graphene-coated Si film is shown in Fig. 5(a), as a function of its thickness d. Note that k monotonically increases as d decreases following nearly the power law $k \propto 1/d$. The thickness dependence of the plasmon thermal conductivity therefore exhibits an opposite behavior to the one of its phonon counterpart (black line) reported for a bare Si membrane at 300 K [33]. $k = 13.6$ W m^{-1} K^{-1} for a Si film at 300 K and a length (thickness) of 5 mm (15 nm). This SPP thermal conductivity represents 67% of its phonon counterpart for a bare Si film [black points in Fig. 5(a)]. As higher k values are obtained for longer or hotter films, the sizable plasmon heat conduction driven by graphene is expected to counterbalance the reduction of the phonon counterpart, as the film length or temperature increases. In terms of the thermal conductance ($G = kad/l$), the SPP contribution is (13.6 W m^{-1} K^{-1}) $\times$ (15 nm) $\times a/l = 204 \times (a/l)$ nW K^{-1}, for a graphene-Si-graphene sandwich at 300 K and a length (thickness) of 5 mm (15 nm). On the other hand, considering that the thermal conductivity of a supported graphene monolayer (thickness ≈ 0.4 nm) lies between 300 and 600 W m^{-1} K^{-1} [34–36], the estimated upper bound for the phonon+electron thermal conductance of the same structure is [(600 W m^{-1} K^{-1}) $\times$ (2 $\times$ 0.4 nm) + (20.3 W m^{-1} K^{-1}) $\times$
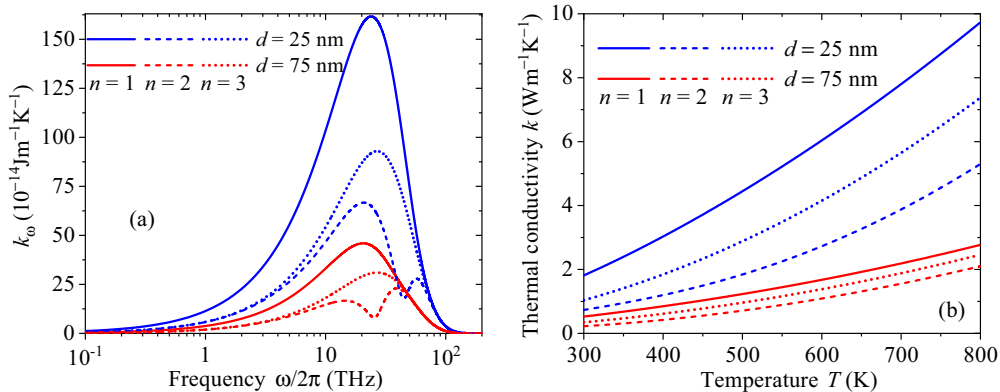

FIG. 4. (a) Spectrum of the SPP thermal conductivity of a 1-mm-long Si film and its (b) integrated counterpart as a function of temperature. Calculations were done for the three SPP modes, two film thicknesses, and $T = 300$ K in (a).
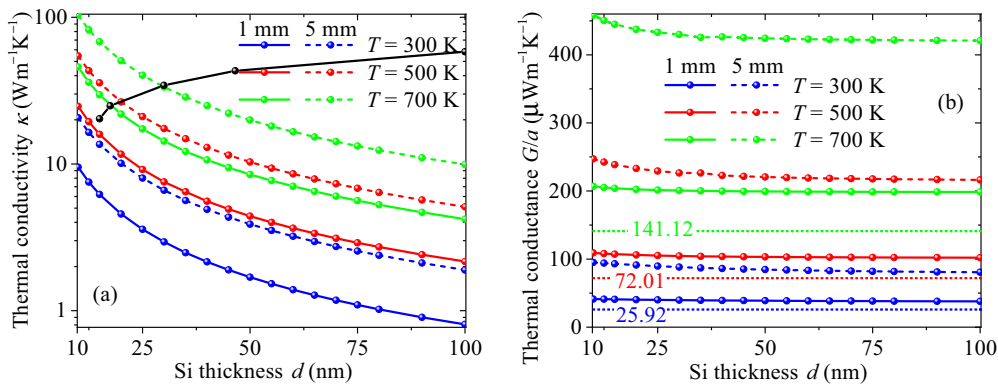
FIG. 5. (a) SPP thermal conductivity and (b) thermal conductance per unit width of a Si film, as functions of its thickness. Calculations were done by summing the contributions of the three SPP modes, for film lengths of 1 and 5 mm, and three representative temperatures. The black points in (a) stand for the phonon thermal conductivity of a suspended Si film at $T = 300$ K [33], while the dotted lines in (b) represent the SPhP quantum of thermal conductance $G_0/a = 12z(3)k_B^3 T^2/ch^2$ of a polar nanofilm [4].

(15 nm)] $\times a/l = 784.5 \times (a/l)$ nW K^{-1}. The SPP contribution to the heat current is therefore $(204/784.5) \times 100\% = 26\%$ of its electron+phonon counterpart. Further, considering that the SPP heat conduction involves the contribution of the long-range mode $n = 3$ [see Fig. 2(b)], which exhibits a ballistic propagation ($l \ll \Lambda$), for any film length of practical interest ($l < 1$ m), its contribution to the SPP thermal conductivity increases linearly with the film length ($k \propto l$), as established by Eqs. (1) and (2). The SPP thermal conductance of this ballistic mode is therefore independent of the film length. Consequently, the SPP contribution to the heat current is expected to become comparable to or even higher than that of phonons and electron, as the sandwich structure length increases. The behavior $k \propto 1/d$ yields a significant SPP thermal conductance nearly independent of the film thickness, as shown in Fig. 5(b). According to Eq. (1), this saturation of G arises from the independence of $\mathrm{Re}(\beta)\Lambda_e$ on d. The opposite dependence on d of the SPP wave vector and propagation length (see Fig. 2) therefore cancels out for each mode and film thickness ($d < 100$ nm) giving significant k values. For a given temperature, G increases with the film length and its values are higher than the maximum one G_0 (dotted lines) supported by a polar nanofilm [4]. This $G > G_0$ results from the combined contribution of three plasmon modes, while G_0 is determined by a single mode supported by polar nanofilms [4]. The graphene coating therefore transforms a Si nanofilm into a plasmonic conductor able to enhance the in-plane heat conduction better than SPhPs in a polar nanofilm, for a given thickness and temperature.

Considering the ultrafast propagation of SPPs, their contribution to the film temperature without the influence of phonons or electrons, could be observed via time-domain thermoreflectance with femtosecond resolution, as done for other structures [37]. Further, the SPP thermal conductivity could

be measured by means of the micro-time-domain thermoreflectance or its steady-state version, which have been used to experimentally probe the polariton thermal conductivity of suspended SiN membranes [10] and supported Ti nanofilms [18], respectively. Whether the SPP heat transport is diffusive or ballistic, it enhances the heat dissipation from a heated spot and therefore lowers its temperature with respect to its value in absence of SPPs. This enhancement is thus expected to allow probing the predicted SPP thermal conductivity by fitting the measured temperature to a proper heat transport model.

In summary, the existence and propagation of three plasmon modes along the interface of a solid film coated with graphene monolayers have been demonstrated. These modes propagate long distances with short wavelengths and speeds close to the one of light in vacuum, which are suitable features to enhance the heat conduction at rates orders of magnitude faster than those of phonons and electrons. A plasmon thermal conductivity of 17 W m^{-1} K^{-1} has been found for a Si film with a thickness of 15 nm, a length of 1 mm, and a mean temperature of 500 K. Higher thermal conductivity values are obtained for thinner, longer, or hotter films. The plasmonic heat conduction driven by graphene could be expanded to other 2D materials and represents an efficient mechanism to offset the thermal performance reduction of dielectric films as their thickness decreases or temperature increases, without changing the internal material structure.

[1] D.-Z. A. Chen, A. Narayanaswamy, and G. Chen, Surface phonon-polariton mediated thermal conductivity enhancement of amorphous thin films, Phys. Rev. B **72**, 155435 (2005).

[2] J. Ordonez-Miranda, L. Tranchant, T. Tokunaga, B. Kim, B. Palpant, Y. Chalopin, T. Antoni, and S. Volz, Anomalous thermal conductivity by surface phonon-polaritons of polar nano

thin films due to their asymmetric surrounding media, J. Appl. Phys. **113**, 084311 (2013).

[3] F. Yang, J. R. Sambles, and G. W. Bradberry, Long-range surface modes supported by thin films, Phys. Rev. B **44**, 5855 (1991).

[4] Y. Guo, S. Tachikawa, S. Volz, M. Nomura, and J. Ordonez-Miranda, Quantum of thermal conductance of nanofilms due to surface-phonon polaritons, Phys. Rev. B **104**, L201407 (2021).

[5] J. Ordonez-Miranda, L. Tranchant, B. Kim, Y. Chalopin, T. Antoni, and S. Volz, Quantized thermal conductance of nanowires at room temperature due to Zenneck surface-phonon polaritons, Phys. Rev. Lett. **112**, 055901 (2014).

[6] V. M. Agranovich, *Surface Polaritons* (Elsevier, Amsterdam, 2012).

[7] D.-Z. A. Chen and G. Chen, Measurement of silicon dioxide surface phonon-polariton propagation length by attenuated total reflection, Appl. Phys. Lett. **91**, 121906 (2007).

[8] J. Ordonez-Miranda, L. Tranchant, T. Antoni, Y. Chalopin, and S. Volz, Thermal conductivity of nano-layered systems due to surface phonon-polaritons, J. Appl. Phys. **115**, 054311 (2014).

[9] L. Tranchant, S. Hamamura, J. Ordonez-Miranda, T. Yabuki, A. Vega-Flick, F. Cervantes-Alvarez, J. J. Alvarado-Gil, S. Volz, and K. Miyazaki, Two-dimensional phonon polariton heat transport, Nano Lett. **19**, 6924 (2019).

[10] Y. Wu, J. Ordonez-Miranda, S. Gluchko, R. Anufriev, D. D. S. Meneses, L. D. Campo, S. Volz, and M. Nomura, Enhanced thermal conduction by surface phonon-polaritons, Sci. Adv. **6**, eabb4461 (2020).

[11] S. Volz, M. Nomura, and J. Ordonez-Miranda, Resonant polariton thermal transport along a vacuum gap, Phys. Rev. Appl. **18**, L051003 (2022).

[12] Y. Wu, J. Ordonez-Miranda, L. Jalabert, S. Tachikawa, R. Anufriev, H. Fujita, S. Volz, and M. Nomura, Observation of heat transport mediated by the propagation distance of surface phonon-polaritons over hundreds of micrometers, Appl. Phys. Lett. **121**, 112203 (2022).

[13] H. Salihoglu, V. Iyer, T. Taniguchi, K. Watanabe, P. D. Ye, and X. Xu, Energy transport by radiation in hyperbolic material comparable to conduction, Adv. Funct. Mater. **30**, 1905830 (2020).

[14] S. Tachikawa, J. Ordonez-Miranda, Y. Wu, L. Jalabert, R. Anufriev, S. Volz, and M. Nomura, In-plane surface phonon-polariton thermal conduction in dielectric multilayer systems, Appl. Phys. Lett. **121**, 202202 (2022).

[15] S. Tachikawa, J. Ordonez-Miranda, Y. Wu, L. Jalabert, R. Anufriev, S. Volz, and M. Nomura, High surface phonon-polariton in-plane thermal conductance along coupled films, Nanomaterials **10**, 1383 (2020).

[16] J. Ordonez-Miranda, Yu. A. Kosevich, B. J. Lee, M. Nomura, and S. Volz, Plasmon thermal conductance and thermal conductivity of metallic nanofilms, Phys. Rev. Appl. **19**, 044046 (2023).

[17] Yu. A. Kosevich, Electrodynamic properties of interface between media and surface electromagnetic waves on a plane defect of a crystal, Zh. Eksp. Teor. Fiz. **96**, 353 (1989) [Sov. Phys. JETP **69**, 200 (1989)].

[18] D.-M. Kim, S. Choi, J. Cho, M. Lim, and B. J. Lee, Boosting thermal conductivity by surface plasmon polaritons propagating along a thin Ti film, Phys. Rev. Lett. **130**, 176302 (2023).

[19] A. A. Balandin, S. Ghosh, W. Bao, I. Calizo, D. Teweldebrhan, F. Miao, and C. N. Lau, Superior thermal conductivity of single-layer graphene, Nano Lett. **8**, 902 (2008).

[20] C. Yu, S. Shan, S. Lu, Z. Zhang, and J. Chen, Characteristics of distinct thermal transport behaviors in single-layer and multilayer graphene, Phys. Rev. B **107**, 165424 (2023).

[21] B. D. Kong, S. Paul, M. B. Nardelli, and K. W. Kim, First-principles analysis of lattice thermal conductivity in monolayer and bilayer graphene, Phys. Rev. B **80**, 033406 (2009).

[22] E. V. Castro, K. S. Novoselov, S. V. Morozov, N. M. R. Peres, J. M. B. Lopes dos Santos, J. Nilsson, F. Guinea, A. K. Geim, and A. H. Castro Neto, Biased bilayer graphene: Semiconductor with a gap tunable by the electric field effect, Phys. Rev. Lett. **99**, 216802 (2007).

[23] M. T. Pettes, I. Jo, Z. Yao, and L. Shi, Influence of polymeric residue on the thermal conductivity of suspended bilayer graphene, Nano Lett. **11**, 1195 (2011).

[24] F. H. L. Koppens, D. E. Chang, and F. J. García de Abajo, Graphene plasmonics: A platform for strong light-matter interactions, Nano Lett. **11**, 3370 (2011).

[25] T. Gu, A. Andryieuski, Y. Hao, Y. Li, J. Hone, C. W. Wong, A. Lavrinenko, T. Low, and T. F. Heinz, Photonic and plasmonic guided modes in graphene-silicon photonic crystals, ACS Photonics **2**, 1552 (2015).

[26] B. Guizal and M. Antezza, Light-induced optomechanical forces in graphene waveguides, Phys. Rev. B **93**, 115427 (2016).

[27] M. Lim, J. Song, S. S. Lee, and B. J. Lee, Tailoring near-field thermal radiation between metallo-dielectric multilayers using coupled surface plasmon polaritons, Nat. Commun. **9**, 4302 (2018).

[28] D.-Z. A. Chen and G. Chen, Heat flow in thin films via surface phonon-polaritons, Front. Heat Mass Transfer **1**, 023005 (2010).

[29] See Supplemental Material at http://link.aps.org/supplemental/10.1103/PhysRevB.108.L161404 for the detailed derivation of the dispersion relation and Poynting vector of SPhPS, as well as the intracavity thermal radiation predicted by Planck's law, which includes a reference to C. Yeh and F. I. Shimabukuro, *The Essence of Dielectric Waveguides* (Springer, New York, 2008).

[30] E. D. Palik, *Handbook of Optical Constants of Solids* (Academic Press, Orlando, FL, 1985).

[31] J. Krupka, J. Breeze, A. Centeno, N. Alford, T. Claussen, and L. Jensen, Measurements of permittivity, dielectric loss tangent, and resistivity of float-zone silicon at microwave frequencies, IEEE Trans. Microwave Theory Tech. **54**, 3995 (2006).

[32] L. A. Falkovsky, Optical properties of graphene, J. Phys.: Conf. Ser. **129**, 012004 (2008).

[33] J. Cuffe, J. K. Eliason, A. A. Maznev, K. C. Collins, J. A. Johnson, A. Shchepetov, M. Prunnila, J. Ahopelto, C. M. Sotomayor Torres, G. Chen, and K. A. Nelson, Reconstructing phonon mean-free-path contributions to thermal conductivity using nanoscale membranes, Phys. Rev. B **91**, 245423 (2015).

[34] W. Cai, A. L. Moore, Y. Zhu, X. Li, S. Chen, L. Shi, and R. S. Ruoff, Thermal transport in suspended and supported

monolayer graphene grown by chemical vapor deposition, Nano Lett. **10**, 1645 (2010).

[35] M. M. Sadeghi, I. Jo, and L. Shi, Phonon-interface scattering in multilayer graphene on an amorphous support, Proc. Natl. Acad. Sci. USA **110**, 16321 (2013).

[36] J. H. Seol, A. L. Moore, L. Shi, I. Jo, and Z. Yao, Thermal conductivity measurement of graphene exfoliated on silicon dioxide, J. Heat Transfer **133**, 022403 (2011).

[37] P. M. Norris, A. P. Caffrey, R. J. Stevens, J. M. Klopf, J. McLeskey, J. T. McLeskey, Jr., and A. N. Smith, Femtosecond pump-probe nondestructive examination of materials (invited), Rev. Sci. Instrum. **74**, 400 (2003).